In-situ SEM and optical microscopy testing for investigation of fatigue crack growth mechanism under overload

Wei Zhang[1,*], *Liang* Cai[2]

[1]Reliability and System Engineering Department, Beihang University, Beijing, China

Abstract. In this paper, the in-situ scanning electron microscope (SEM) and optical microscopy experiments are performed to investigate the crack growth behavior under the single tensile overload. The objectives are to (i) examine the overload-induced crack growth micromechanisms, including the initial crack growth acceleration and the subsequent retardation period ; (ii) investigate the effective region of single overload on crack growth rate. The specimen is a small thin Al2024-T3 plate with an edge-crack, which is loaded and observed in the SEM chamber. The very high resolution images of the crack tip are taken under the simple variable amplitude loading. Imaging analysis is performed to quantify the crack tip deformation at any time instant. Moreover, an identical specimen subjected to the same load condition is observed under optical microscope. In this testing, fine speckling is performed to promote the accuracy of digital imaging correlation (DIC). The images around the crack tip are taken at the peak loads before, during and after the single overload. After that, the evolution of local strain distribution is obtained through DIC technique. The results show that the rapid connection between the main crack and microcracks accounts for the initial crack growth acceleration. The crack closure level can be responsible for the crack growth rate during the steady growth period. Besides that, the size of retardation area is larger than the classical solution.

1 Introduction

Many structural components are usually subjected to the moderate amplitude fatigue loading with occasional large spike loads, which can be simplified as constant amplitude loading with overloads. Many studies claim that the applied overload can lead to the typical nonlinear crack propagation, which includes instant crack growth rate acceleration, a long-time crack growth retardation and sometimes even crack arrest[1-4]. It is essential to understand the exact fatigue crack growth mechanism under the constant amplitude load with overload. A great amount of theoretical and experimental explorations proposed in the past to investigate mechanism of the transient acceleration and the following retardation period [5-9]. Among them, the crack closure concept proposed by Elber [10] is widely recognized in which the effective stress intensity factor is considered as the unique driving force of the crack growth. Crack closure is successfully used to explain the retardation phenomenon [11]. Some researchers use the crack closure to explain the post-overload transient acceleration [12,13]. They claim that the overload-induced enlarged plastic zone leads to crack tip blunting, which causes the concentration of high stress. However, the increase of effective stress intensity factor cannot fully accounts for the acceleration phenomenon, which makes the crack closure theory controversial. Many studies use the plasticity and residual stress to investigate the overload effect on fatigue crack growth. For instance, Willenborg et al. described the retardation phenomenon by proposing a relationship between the effective stress intensity factor and the plastic zone size [14]. However, the transient acceleration period is not taken into account in their model. Besides, their models are based on the assumption of monotonic plastic zone without consideration of the effect of residual stress by the previous loading sequence and the shape of the large plastic zone. In addition, the overload ratio for crack arrest equals to 2 according to Willenborg's model. However, many experimental results show that this value is greater than 2 in the actual situation [15]. Although, many studies are proposed to modify Willenborg's model [16-18], there is still a lack of convincing experimental observation. Therefore, a reliable approach to determine the crack closure level and the failure phenomenon is important to understand the crack tip driving force under variable amplitude load.

In this paper, an in-situ SEM fatigue testing approach is proposed to directly observe the crack closure within one loading cycle and the transient acceleration under single overload case. Meanwhile, an investigation of the plastic zone evolution near the fatigue crack tip is carried out to assist the examination of fatigue crack growth mechanism.

2 Experimental setup and specimen design

* Corresponding author: zhangwei.dse@buaa.edu.cn

© The Authors, published by EDP Sciences. This is an open access article distributed under the terms of the Creative Commons Attribution License 4.0 (http://creativecommons.org/licenses/by/4.0/).

Two different experimental approaches are applied in the current studies: an in-situ scanning electron microscope (SEM) testing and an in-situ optical microscopy testing. The in-situ SEM experiment is conducted to investigate the overload-induced crack growth micromechanisms by analyzing the high resolution images taken around the fatigue crack tip. The detailed illustration of the experimental setup is shown in Fig.1. It mainly includes a palm-sized load stage installed in a field emission SEM (FEG 650), inside of which a secondary electron beam is applied. The load stage has a maximum load capacity of 5kN. The specimen is clamped on the load stage and cyclic load is applied during the testing. The vacuum level remains lower than 3×10^{-2} MPa. The working distance is approximately between 15 to 20 mm. A desktop is used to monitor the deformation process near the crack tip and collect those images taken under the SEM.

Fig.1. Experimental setup of in-situ SEM testing (a) and the load stage installed in SEM (b)

The specimen is a single edged notch plate made of aluminum alloy sheet (Al2024-T3), as shown in Fig.2. Its width *W* is 10 mm, length *L* is 32 mm and thickness *T* is 1.02 mm. The edged notch of 1mm is machined by low speed wire-cutting electronical discharge machining (LSWEDM) for efficient avoidance of the residual stress in this cutting process. After that, the specimen is pre-cracked under a low stress level using an electromagnetic fatigue loading machine M-3000. Following this, the specimen with an initial crack is polished by using a metallographic polishing machine (1 um polishing suspension in the final step), which facilitates the observations of the crack tip deformation. The mechanical properties of Al2024-T3 are given in table 1.

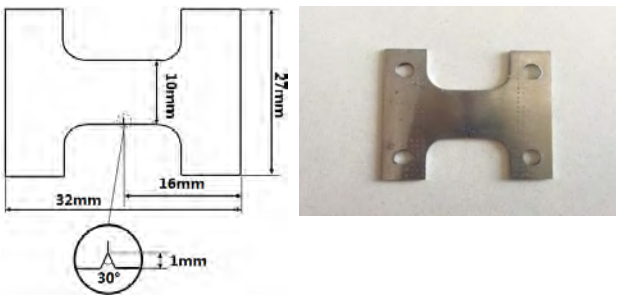

Fig. 2. The illustration the specimen geometry and specimen configuration

Table.1. mechanical properties of Al2024-T3

Ultimate tensile strength	453-459 MPa
Tensile yield stress	306-310 MPa
Young's Module	71.7 GPa

3 Experimental procedure and analysis

3.1 In-situ SEM testing

3.1.1 Experimental procedures

Tensile-tensile cyclic load is applied on the specimen and the crack growth behavior is monitored in-situ under the SEM. The overloading spectrum includes a constant amplitude loading part (the maximum loading 1.5kN and the minimum loading 0kN), and a single spike load with an overload ratio of 1.2. Firstly, the 30-50 cycles of loading is applied on the specimen to ensure the steady growth of the crack tip. Then, the crack tip deformation is traced before, during and after the single overload. Two major characteristics are measured: crack tip opening displacement (CTOD) and the crack growth. The CTOD under the constant amplitude load is defined as the opening displacement at the previous crack tip location. During the CTOD measurement, the load cycle is divided into many steps. When the stress level remains stable at each step, the images in the vicinity of the crack tip are taken under very high magnification. Reference points on the crack surface are chosen to ensure that the images are collected in-situ. The images taken during the loading process within one load cycle before overload are shown in Fig.3. The yellow lines represent the current crack tip positions and the horizontal brackets indicate the CTOD.

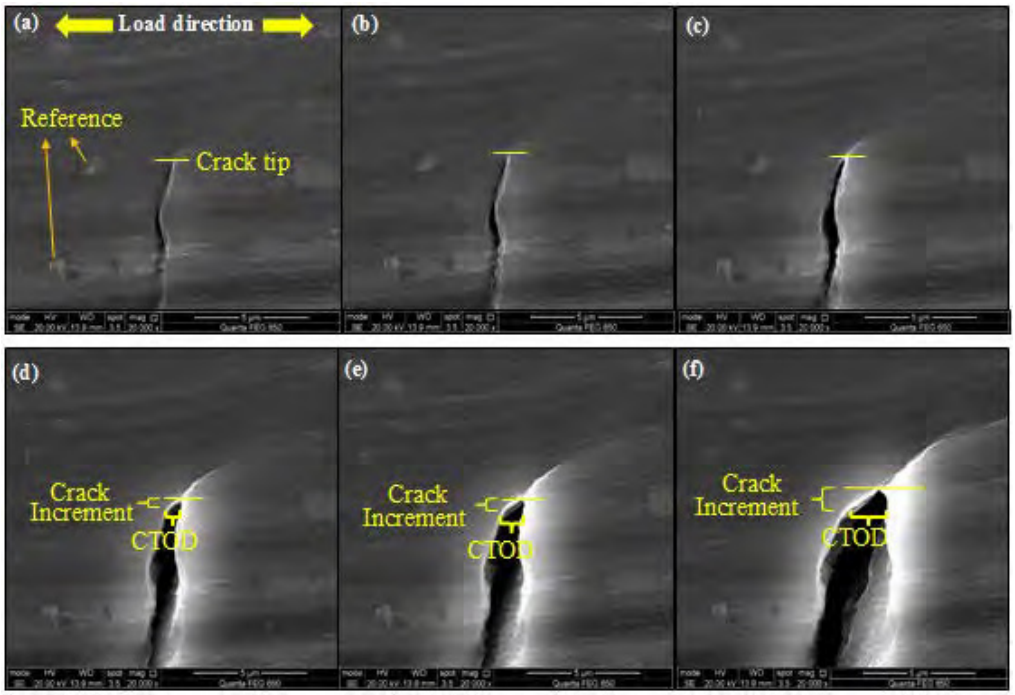

Fig.3. Illustration of CTOD measurements under different load levels during the retardation period (from a to f: K=0, 2.4, 4.8, 7.3, 9.7, 12.1Mpa•m$^{0.5}$, magnification 20000x)

The crack growth rate is defined as the crack increments between two maximum loads within one load cycle, where the crack increments are quantified by measuring the distance of the new crack tip to the original crack tip along the crack direction. The micrographs of crack tip at maximum load are taken cycle by cycle before the overload, shown in Fig.4. It is clearly seen that the fatigue crack tip produce a steady crack growth rate under constant amplitude load.

Fig. 5 shows the SEM micrographs near the crack tip at maximum load before and during the overload (Fig.5b and Fig.5c), and in the unloaded condition before overload (Fig.5a) and immediately after overload (Fig.5d). It is found that the CTOD significantly increases and plenty of shear bands appear in front of the crack tip during the overload. The crack tip is completely closed at unloaded condition before overload, whereas the crack blunting is found in the same loading condition right after the overload.

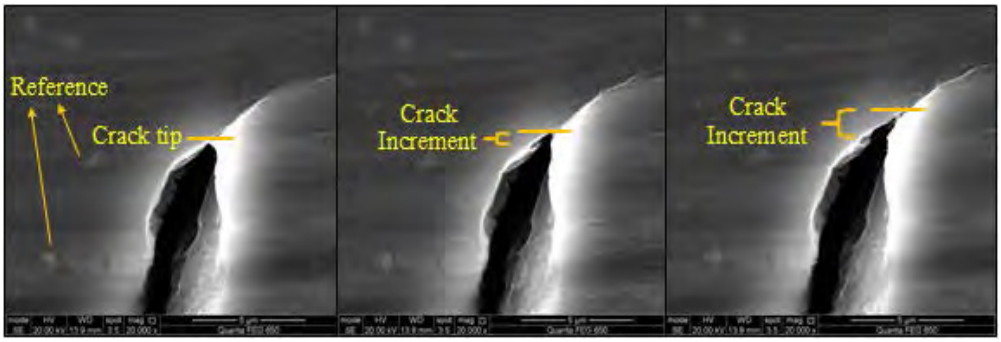

Fig.4. Crack increments at three consecutive peak loads before overload (magnification 20000x)

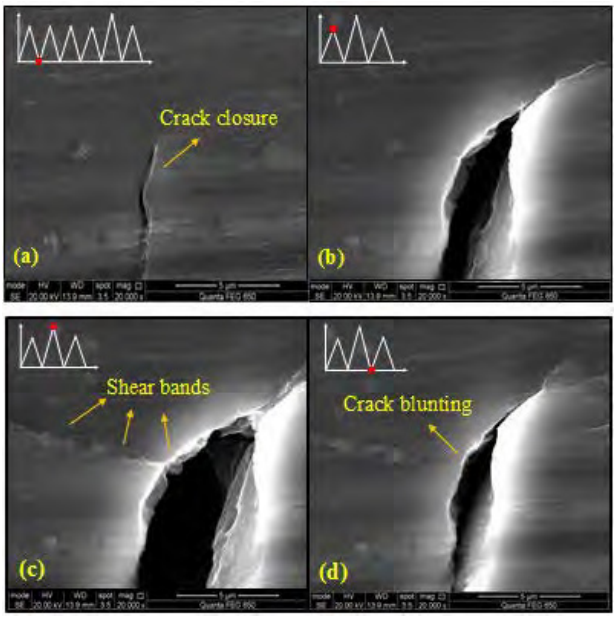

Fig.5. SEM micrograph: (a) minimum load before overload; (b) maximum load before overload; (c) maximum load during overload;(d) minimum load right after overload (magnification 20000x)

Fig.6 gives the crack tip behavior at maximum load immediately after the single overload. The magnification is adjusted to 5000x. It can be seen that the shear bands in Fig.6(c) develop into microcracks rapidly right after the overload. Then the microcracks connect with the main crack and produce a fast crack growth rate within several load cycles, as shown in Fig.6 (a)-(c). It is also found the crack tip usually tends to bifurcates after the overload. The main crack propagates along one of these two directions. Subsequently, a long-time crack growth retardation is observed. Fig.6 (d) illustrates the crack tip that just enters the retardation period. The crack growth rate during the acceleration period is calculated by the ratio of the entire crack increments during this whole period to its corresponding load cycles.

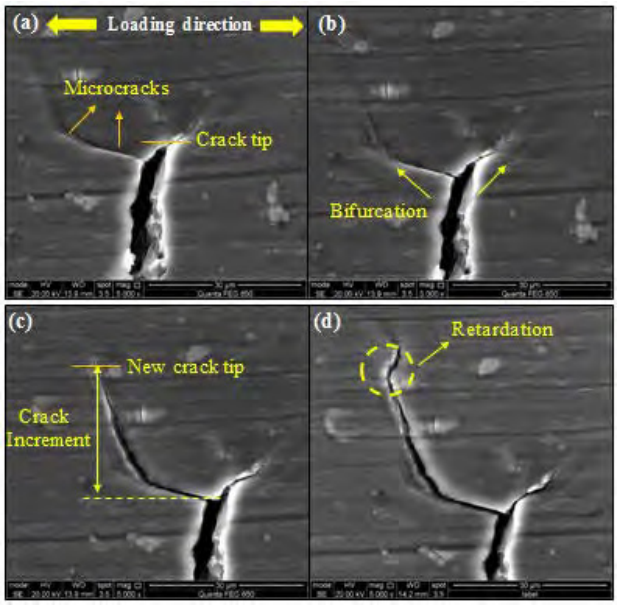

Fig.6. The crack tip behavior at maximum loading within several load cycles immediately after overload (magnification 5000x)

The illustrations of the crack tip deformation from the minimum load to the maximum loading within one load cycle during the retadation period are shown in Fig.7(a)–7(f). The measuring position corresponds to the yellow circle in Fig.6 (d). It is observed that no evident crack growth is found in one loading cycle during this period. Therefore, the CTOD is defined as the opening displacement with a measurement distance identical to that under the same load value before overload. Take Fig.7 (f) as an example, the measurement distance *a* is equal to the crack increment indicated in Fig.3 (f).

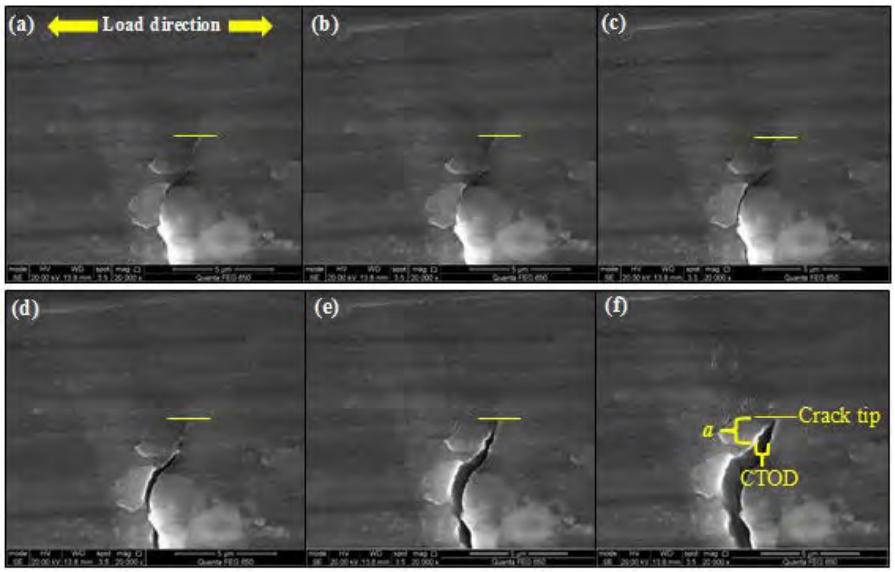

Fig.7. Illustration of CTOD measurements under different load levels during the retardation period (from a to f: K=0, 2.4, 4.8, 7.3, 9.7, 12.1, magnification 20000x)

Due to the overload-induced crack growth retardation, the crack increments are measured every ten load cycles in order to reduce the error. Fig.8 shows the two images of crack tip between two adjacent measuring position with an interval of ten load cycles. It is clearly seen that the crack growth rate decrease to approximately 0.2um/cycle.

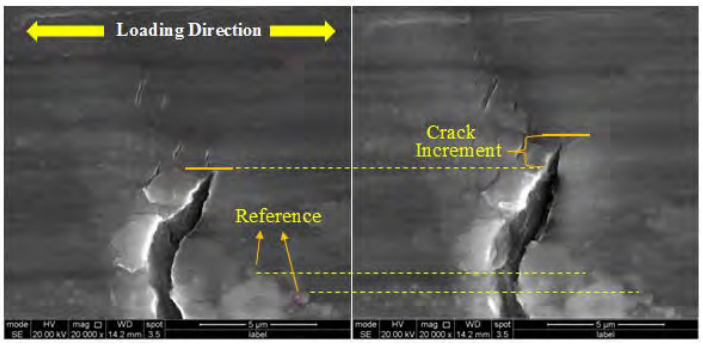

Fig.8. The crack increments between two adjacent measuring position during the retardation period (magnification 20000)

3.1.2 Analysis of experimental results

For the constant amplitude load part, it is observed the CTOD at peak load of one cycle before overload is approximately 2.5um and this value decrease to 1.2um at the beginning of the retardation period. The CTOD is correlated with the effective stress intensity factor(SIF) range modified by the crack closure level[19], given in equation (1). The equation (2) gives the relationship between effective SIF and crack growth rate[20]. Equation (3) can be drawn from equation(1) and (2).

$$CTOD = \begin{cases} \frac{1}{2\alpha}\left(\frac{K-K_{op}}{E\sigma_y}\right)^2 & K > K_{open} \\ 0 & K \le K_{open} \end{cases} \quad (1)$$

$$\frac{da}{dN} = C(K-K_{op})^m \quad (2)$$

$$\frac{da}{dN} = C'(CTOD)^{\frac{m}{2}} \quad (3)$$

In the current experiment, the measured crack growth rate before overload and during the retardation period is plotted against its corresponding CTOD in logarithmic coordinate, shown in Fig.9. It is seen that they exhibit line relationship under the logarithmic coordinate, where *m* approximately equals to 3 according to the slope. This indicates that CTOD can be used to estimate the crack growth rate. In other words, the crack growth rate can be reflected by the crack closure level.

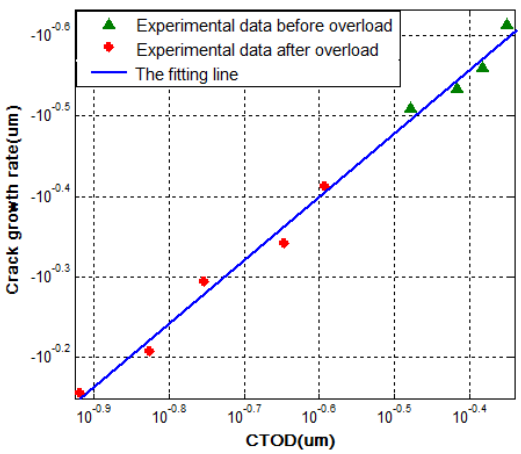

Fig.9. CTOD vs. crack growth rate in the single tensile overload case

The crack growth rate in the current overload case is plotted against the load cycles in Fig.10. The steady crack growth rate before overload is approximately 0.6 um/cycle. The single overload is applied on the specimen at 290th load cycles. The crack growth rate during the post-overload acceleration period is reaches 3.1 um/cycle. After that, the crack growth rate decreases sharply and experiences a long-time retardation. The trend of crack growth rate without overload are visualized as the green line by using linear fit of the experimental data acquired before overload. As the crack continues to advance, the crack growth rate in the sample cycles shows a gradual restoration to the trend before the spike load at approximately 1220th load cycles. The crack increment from the recovery position to the overload site is approximately 430 um according to the experimental measurement.

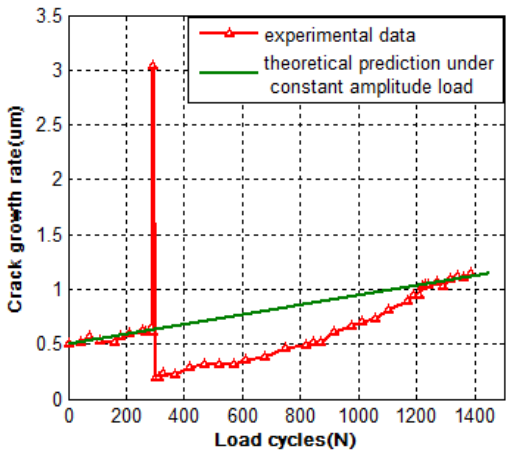

Fig.10. Load cycles vs. crack growth rate in the single tensile overload case

The theoretical predictions for the diameter of the forward plastic zone considering the crack closure effect can be expressed as

$$\rho_f = \begin{cases} \frac{1}{\pi}\left(\frac{K-K_{op}}{\sigma_y}\right)^2 & K_{max} \ge K > K_{op} \\ 0 & 0 \le K \le K_{op} \end{cases} \quad (2)$$

* Corresponding author: zhangwei.dse@buaa.edu.cn

$$K = F \times \sigma\sqrt{\pi a} \quad (3)$$

$$F = 1.12 - 0.23 + 10.6\left(\frac{a}{W}\right) - 21.7\left(\frac{a}{W}\right)^3 + 30.4\left(\frac{a}{W}\right)^4 \quad (4)$$

The diameter of the overload-induced enlarged forward plastic zone in current study equals to 403 um by using equation (2), which is slightly less than the experimental results of the distance from the crack growth rate recovery position to the overload site.

3.2 In-situ optical microscopy testing

In our previous study, an equivalent specimen subjected to the same load condition is observed under optical microscope. The experimental set-up for the in-situ optical microscopy testing is shown in Fig.11, which mainly includes: an in-situ fatigue testing stage, an optical measuring microscope, and an imaging processing system. The loading stage is installed on the platform of measuring microscope, whose magnification is adjusted to 50x. The tested specimen is fixed on the stage and cyclic loading is applied on the specimen. A microscopy camera is used to acquire the images in high resolution during the loading process. Afterwards, these images are collected and processed by digital imaging correlation (DIC) system.

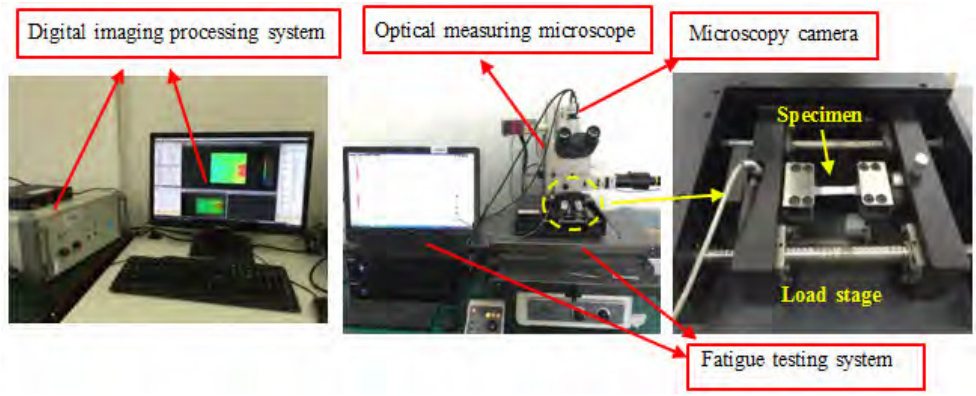

Fig.11 The experimental set-up of in-situ optical microscopy testing

In this testing, the specimen surface is speckled with tiny dense spots to improve the accuracy of DIC. For the measurement of strain distribution, the images of the crack tip taken at the previous minimum loads are set as reference and the image taken at current maximum load are compared with it. The distance from the crack tip to the plastic zone boundary along the crack direction is defined as the diameter of the plastic zone. The strain at boundary of the plastic zone is approximately equal to yield strain. Once the strain distribution along the diameter direction is averaged measured, the diameter can be easily determined.

The strain evolution in the vicinity of the crack tip under the single overload are acquired and measured. The strain contours near the fatigue crack tip at maximum loads before, during and right after the overload are given in Fig.12 (a)-(c), where the white line indicates the crack tip position. It is can be seen that plastic zone near the crack tip dramatically declines right after overload, compared with that before overload under the same loading condition. The variations of plastic zone at the maximum loads and the corresponding crack increments are measured every one hundred cycles after the single overload. It is observed that, as the fatigue crack advanced, the plastic zone size gradually recovers to the level before the overload. Fig.12 (d) shows the restoration of plastic zone at the 2000th load cycle after the spike load.

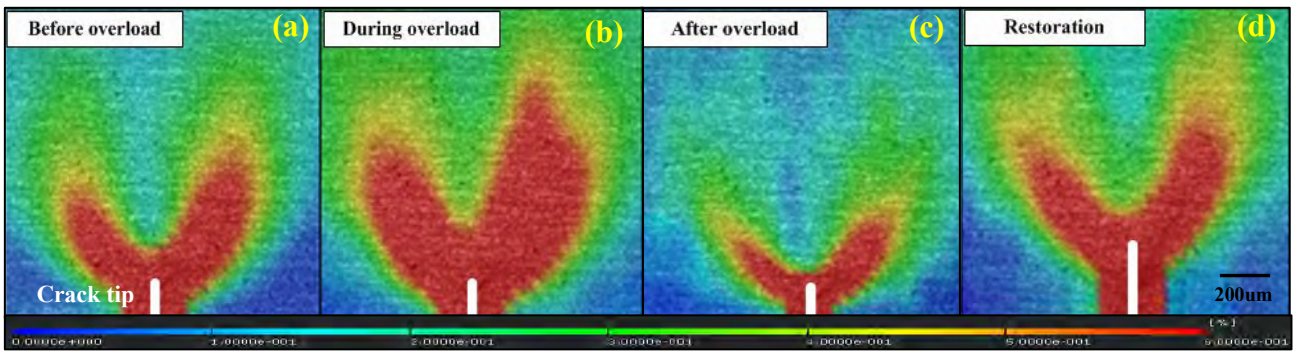

Fig.12 The strain evolution near the crack tip at maximum loading in overload case (from left to right: before, during, right after the overload and 2000th after overload)

The evolution of plastic zone size during the whole single overload case is plotted against the crack growth in Fig.13. It is observed that after the single overload, the plastic zone size returns to the original level before overload until the crack growth reaches 280 um. This distance is almost equal to the diameter of large plastic zone caused by the single overload.

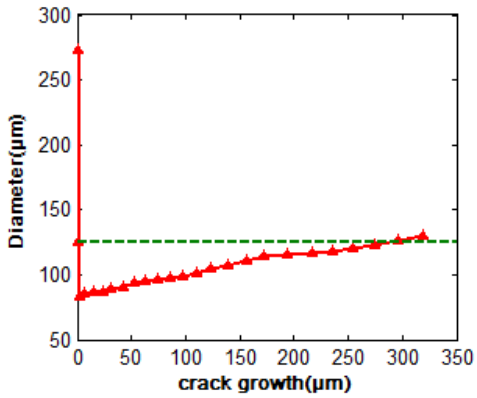

Fig.13 Crack growth vs. measured plastic zone diameter

4 Discussions

Based on the experimental results and analysis, it is found that the CTOD can be used to estimate the crack growth rate during the steady growth stage, which suggests that the crack closure level can be a dominant parameter of the crack growth rate.

There is no crack closure in the unloaded condition immediately after the overload, which might contribute to the initial acceleration due to the high stress concentration in the crack blunting region. However, the crack growth rate is 5 times than that of this value in the steady growth period before overload. The increase of effective stress intensity factor cannot fully accounts for the post-overload transient acceleration. Another micromechanism might be due to the overload-induced enlarged plastic deformation ahead of the fatigue crack tip, shown in Fig.12 (b), which produces a great number of shear bands, microcracks and potential damage. Then, the rapid connection of the microcracks and the primary crack generates a fast crack growth rate. The crack bifurcation caused by the single tensile overload may also reduce the stress intensity factor of each crack tip, which contributes to the crack growth retardation.

As for most of the plasticity-based models describing the crack growth retardation, it is supposed that once the current plastic zone reaches the boundary of large plastic zone, the retardation phenomenon vanishes [11,21,22,23]. However, according to the experimental observations in the SEM and optical microscopy testing, both of the crack growth rate recovery location and the plastic zone restoration position are further away from the overload site than the classical solution. This phenomenon is probably related with the shape effect of the large plastic zone, which is not taken into account in those classical plasticity-based models.

5 Conclusions and future work

In this paper, in-situ SEM and optical microscopy testing are performed to investigate the fatigue crack growth mechanism under the single overload. The SEM experiment successfully investigated the micromechanism of the transient crack growth acceleration and the following retardation period. Both the in-situ SEM and optical testing results suggest a revision of the classical plasticity-based retardation model. Several conclusions are drawn based on current study.

- The crack closure is considered as a dominant parameter of the crack growth rate in the steady growth stage.
- The rapid coalescence of the microcracks with the primary crack is a significant mechanism for transient acceleration right after the overload. The decrease or vanishing of the crack closure caused by large plastic deformation of the crack tip cannot fully explain this transient acceleration.
- The crack bifurcation caused by the single tensile overload contributes to the crack growth retardation.
- The actual region of retardation is larger than the assumption of classical solution. The shape effect of the large plastic zone probably contributes to this phenomenon, which is ignored in the classical models

In the future, the overload-induced crack growth micromechanisms of different metallic materials will be investigated. Besides, multiple overload ratio cases, even the crack growth arrest, need further exploration.

Acknowledgements

This research reported in this paper was financially supported by National Natural Science Foundation of China (No. 51405009).

References

1. Damri. D, Knott, J.F. Fatigue & Fracture of Engineering Materials & Structures, **14(7)**, 709-719 (1991)
2. Seifi R, Bahrami R. Engineering Failure Analysis, **17(6)**,1475-1482(2010).
3. Corbly D M, Packman P F. Engineering Fracture Mechanics, **5(2)**, 479-497(1973).
4. Rao K T V, Ritchie R O. Acta Metallurgica, **36(10)**, 2849-2862(1988)
5. Newman, J. C. Astm Stp, 1981.
6. Bichler C, Pippan R. Engineering Fracture Mechanics, **74(8)**, 1344-1359(2007).
7. Borrego L P, Ferreira J M, Cruz J M P D, et al. Engineering Fracture Mechanics, **70(11)**, 1379-1397. (2003)
8. Robin C, Pelloux R M. Materials Science & Engineering, **44(1)**, 115-120(1980)
9. Elber W. Astm Stp, 486(1971).

10. Yang J, Zhang W, Liu Y. International Journal of Fatigue, **62(2)**, 144-153(2014).
11. Lee S Y, Liaw P K, Choo H, et al. Acta Materialia, **59(2)**: 485-494(2011).
12. Lee S Y, Choo H, Liaw P K, et al. Acta Materialia, **59(2)**, 495-502(2011).
13. J. Willenborg, R.M. Engle, H.A. Wood, 1971.
14. Manjunatha M, Parida B K., **42(8)**:1536-1542. (2004)
15. Ziegler B, Yamada Y, Jr J C N., **78(14)**, 2609-2619. (2011)
16. Sun G, Chen J. Journal of Mechanical Strength, **10(2)**, 161-173(1992).
17. Ray A, Patankar R. Applied Mathematical Modelling, **25(11)**, 979-994(2001).
18. Ray A, Patankar R. Applied Mathematical Modelling, **25(11)**, 995-1013(2001).
19. Zhang W, Liu Y. International Journal of Fatigue, **42(4)**,14-23(2012).
20. P.C. Paris, F. Erdogan, Journal of Basic Engineering, **85(4)**,528-533(963).
21. O.E. Wheeler, **94(1)**, 181–186.2(1972)
22. B.K.C. Yuen, F. Taheri, International Journal of Fatigue, **28(12)**, 1803-1819(2006).
23. M.V.S. Pereira, F.A.I. Darwish, A.F. Camarão, et al. Materials Research, **10(2)**, 101-107(2007).